Lateral flexural vibration reduction in a periodic piping system enhanced with 2DoF resonator

Journal:	*Part L: Journal of Materials: Design and Applications*
Manuscript ID	JMDA-21-0149
Manuscript Type:	Special Issue: Metamaterials: Design, Modelling, Simulation and Implementation
Date Submitted by the Author:	14-Mar-2021
Complete List of Authors:	Iqbal, Mohd; Indian Institute of Technology Roorkee, Mechanical and Industrial Engineering KUMAR, ANIL; Indian Institute of Technology Roorkee, Mechanical and Industrial Engineering Bursi, Oreste; University of Trento Department of Civil Environmental and Mechanical Engineering
Keywords:	wave propagation, periodic piping system, propagation constant, band gap, locally resonant
Abstract:	Pipe systems are commonly used in the process and power industries to transport fluid from one terminal to others. Propagation behaviour of lateral flexural waves in a pipe coupled with periodic rack structure is investigated. The pipe-rack system considered in this study is a practical case and is realized as a pipe on periodic elastic supports, while a pipe on simple and without supports represent the special cases when the rack stiffness leads to extreme values. The propagation constant relations in term of frequency are derived using Bloch-Floquet theorem which are successively verified with finite element models. A pipe over rack exhibits a locally resonant band gap around first natural mode of the rack. Conversely, a pipe on simple supports entails only Bragg type band gaps, while a pipe without supports carries no band gap. For tuning the band gap properties, a two-degree-of-freedom (2DoF) lateral localized resonator in series is attached to the center of each unit cell of the pipe. It is found that the targeted pass bands are effectively controlled. Further, the effect of various resonator parameters, i.e. mass ratio, stiffness and damping, on band gaps is examined. It is observed that the band gaps are vanished when damping is introduced in the system. The results show a promising way to flexural vibration control of a periodic piping system with various boundary conditions.

Lateral flexural vibration reduction in a periodic piping system enhanced with 2DoF resonator

Mohd Iqbal[a], Anil Kumar[b*] and Oreste Salvatore Bursi[c]

[a]PhD Student, Department of Mechanical and Industrial Engineering, Indian Institute of Technology Roorkee, Roorkee, 247667, India.

[b]Associate Professor, Department of Mechanical and Industrial Engineering, Indian Institute of Technology Roorkee, Roorkee, 247667, India.

[c]Professor, Department of Civil, Environmental and Mechanical Engineering, University of Trento, Trento, 38123, Italy.

*Email: anil.kumar@me.iitr.ac.in

Abstract

Pipe systems are commonly used in the process and power industries to transport fluid from one terminal to others. Propagation behaviour of lateral flexural waves in a pipe coupled with periodic rack structure is investigated. The pipe-rack system considered in this study is a practical case and is realized as a pipe on periodic elastic supports, while a pipe on simple and without supports represent the special cases when the rack stiffness leads to extreme values. The propagation constant relations in term of frequency are derived using Bloch-Floquet theorem which are successively verified with finite element models. A pipe over rack exhibits a locally resonant band gap around first natural mode of the rack. Conversely, a pipe on simple supports entails only Bragg type band gaps, while a pipe without supports carries no band gap. For tuning the band gap properties, a two-degree-of-freedom (2DoF) lateral localized resonator in series is attached to the center of each unit cell of the pipe. It is found that the targeted pass bands are effectively controlled. Further, the effect of various resonator parameters, i.e. mass ratio, stiffness and damping, on band gaps is examined. It is observed that the band gaps are vanished when damping is introduced in the system. The results show a promising way to flexural vibration control of a periodic piping system with various boundary conditions.

Keywords

wave propagation, periodic piping system, propagation constant, band gap, locally resonant

Introduction

Fluid-conveying pipes are widely used in petrochemical plants, liquefied natural gas (LNG) plants and various engineering applications. Long pipelines are very common in such plants. A large-amplitude vibration in pipelines due to the opening/closing of a valve, flow pulsation and support excitation can cause fretting, loosening of joints and fatigue failure. Hence, it is important to study both lower and higher vibration modes in pipe systems[1,2], based on which an efficient vibration control strategy can be developed.

A structure with repetitive units is designated as the periodic structure. Propagation behaviour of

elastic waves in periodic structures has been investigated for decades[1,3,4]. Meanwhile, the idea of phononic crystals (PCs) introduced from solid-state physics unveils a new direction to investigate the motion of acoustic/elastic waves in periodic structures. Conversely to traditional periodic structures, PCs are the classy periodic composite materials which generally possess the boundary, geometry or material type periodic spatial variation. Due to existence of any such variation, PCs show distinctive characteristics of band gaps, which can forbid both sound and vibration. Two types of mechanisms are responsible for the formation of these band gaps: Bragg scattering mechanism[3,5] and locally resonant (LR) mechanism[6]. As a result, few waves freely propagate in a specific frequency range and result in pass bands while remaining waves attenuate and create band gaps or stop bands. If the lattice constant l and wavelength β are of the same order, the structure results in Bragg type band gaps. Frequencies of such band gaps are determined by Bragg condition $l = n\left(\frac{\beta}{2}\right)$, where $n = 1, 2, 3, ...$The earlier investigations relevant to propagation of elastic wave in periodic beam[4,7], pipes[1,2], plates[3], skin-stringer/rib-skin structures[8] were based on the Bragg scattering mechanism.

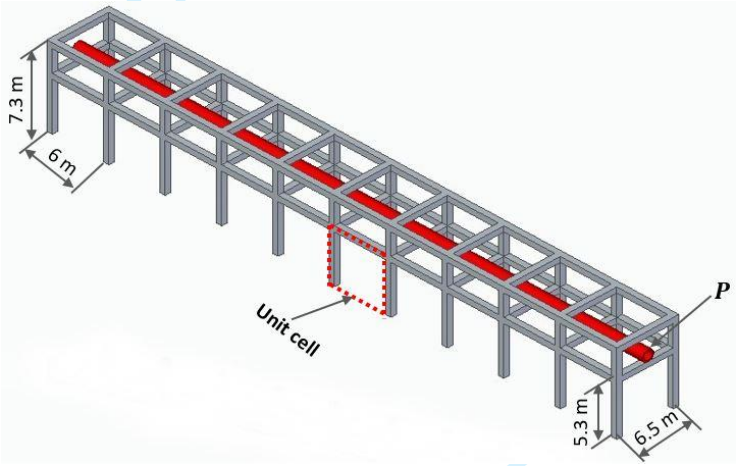

Figure 1. The periodic rack structure with a pipe P.

Conversely to conventional Bragg band gaps, Liu et al.[6] proposed that the band gaps in PCs can be achieved at low frequency regime by means of LR mechanism if l is of two order lower magnitude than the relevant wavelength β. Owing to negative effective properties, LR PCs are classified as acoustic/elastic metamaterials[9], and has received considerable attention from the research community in the recent decade.

Most of the previous studies relevant to LR periodic structures are focused on single-degree-of-freedom (SDoF) resonator. Recently, vibration band gaps in metamaterial pipes[10–12], beams[13–15], shafts[16,17] and rod[18] were studied using SDoF resonator. Yu et al.[10] investigated LR pipe with different lattice constant and obtained resonance and Bragg type stop bands, and concluded that LR pipe with a large lattice constant entails Bragg band gap at lower frequency range than LR band gap. However, the study on propagation of elastic waves in beam[19] and rod[20] was conducted when a multiple-degrees-of-freedom (MDoF) resonator was used. Such structures with LR units evolve additional band gaps near the resonant frequency thereby wave filtering capability of the structure can be enhanced.

In this study, the propagation characteristic of lateral flexural wave in a pipe *P* supported on a rack is investigated theoretically and numerically. In this regard, three models are considered: i) a pipe over flexible supports (i.e., a pipe coupled with rack) - Model #A-; ii) a pipe over simple supports - Model #B-; and iii) a pipe without any support – Model #C-. Pipe over elastic supports represents a realistic case, while other two models approximate the extreme scenarios. The equivalent models of Figure 1 are shown in Figure 2 for the cases when Model #A is without resonators and with 2DoF resonators. In order to derive the dispersion relation for Model #A, Bloch-Floquet theorem of periodic structure is used. The analytical results are successively verified by FE models.
In addition, a 2DoF resonator is periodically attached with the pipe to tune the band gap properties as depicted in Figure 2(b). In order to perform these studies, a FE model is developed whose accuracy is confirmed with the analytical results. Moreover, the parametric study based on the resonator properties is conducted to know their influence on the position and width of band gaps. Finally, the main findings are concluded at last.

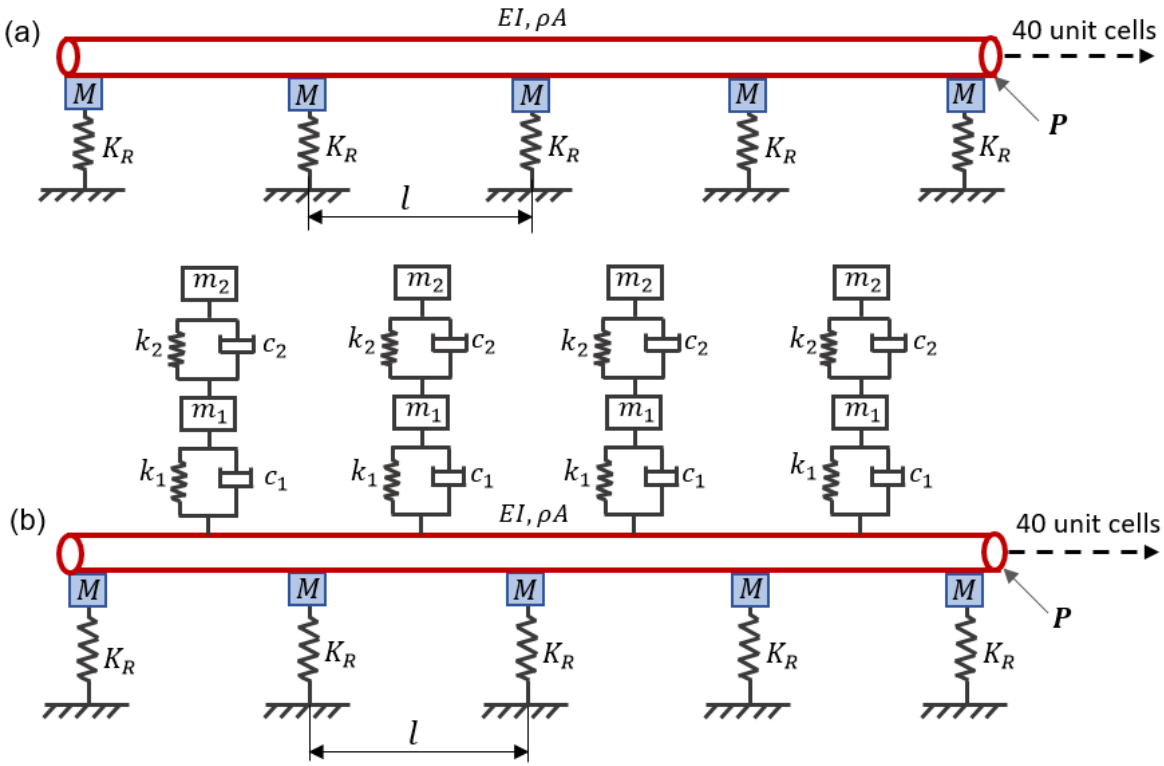

Figure 2. Simplified models of a pipe *P* for Figure 1, i.e. *P* over flexible supports: (a) *P* without resonators; and (b) a 2DoF resonator is attached at the mid of each unit span of *P*.

Band gaps in a periodic piping system

Analytical modelling of an infinite periodic piping system

The simplified model of a coupled-pipe rack system depicted in Figure 2(a) is used to investigate the propagation behaviour of lateral flexural wave in pipe *P*. Two unit cells shown in Figure 3 (a)

are used to formulate the dispersion relation. The undamped pipe P is modelled as Euler- Bernoulli beam whose governing equation of motion is expressed by,

$$\frac{\partial^2}{\partial x^2}\left[EI\frac{\partial^2 y(x,t)}{\partial x^2}\right]+\rho A\frac{\partial^2 y(x,t)}{\partial t^2}=0 \tag{1}$$

where E, ρ, A and I respectively denotes modulus of elasticity, mass density, area of cross-section and inertia moment. y is the transverse displacement. The substitution of harmonic solution $y(x,t)=Y(x)e^{i\omega t}$ in equation (1) yields,

$$EIY^{iv}(x)-\rho A\omega^2(x)=0 \tag{2}$$

where ω is the radian frequency and $Y(x)$ is beam displacement amplitude. The solution of equation (2) yields the beam displacement as,

$$Y(x)=A\cos(\lambda x)+B\sin(\lambda x)+C\cosh(\lambda x)+D\sinh(\lambda x) \tag{3}$$

here $\lambda=\left(\frac{\rho A\omega^2}{EI}\right)^{\frac{1}{4}}$ represents flexural wavenumber of the beam.

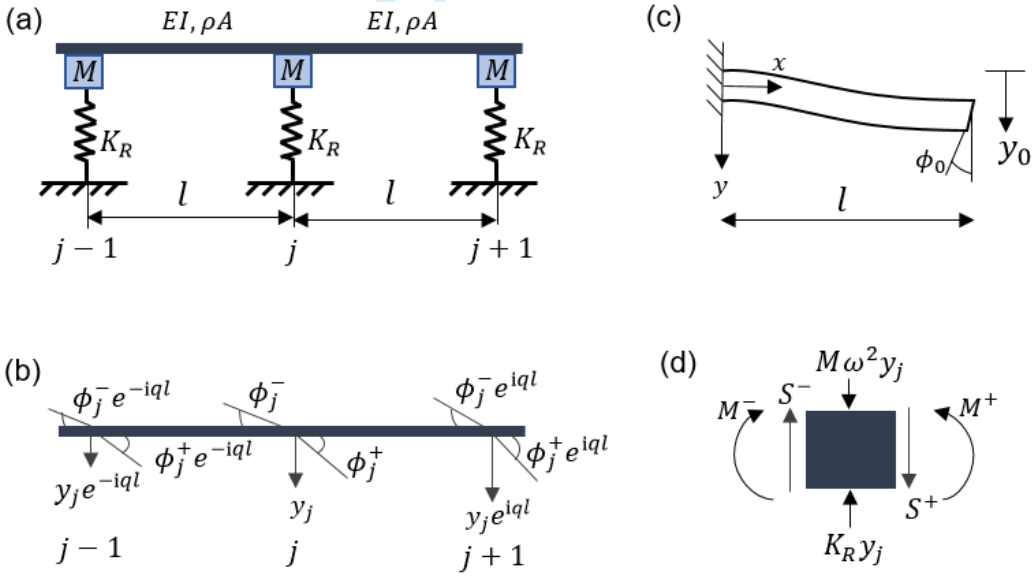

Figure 3. Analytical modelling of P: (a) two unit cells of P on elastic supports; (b) Bloch- Floquet theory imposed at the generic node j for angular and transverse displacements; (c) single span of P illustrated as a beam with transverse displacement y_0 and rotation ψ_0 at free end and clamped at other end; and (d) equilibrium of forces and bending moments balance at node j.

Applying Bloch- Floquet theorem[21,22] to the generic nodes of each unit cell depicted in Figure 3(b), the transverse and angular displacements of nodes $j-1$ and $j+1$ with node j are associated as

$$y_{j-1}=y_je^{-iql},\ y_{j+1}=y_je^{iql}\ \text{and}\ \phi_{j-1}=\phi_je^{-iql},\ \phi_{j+1}=\phi_je^{iql} \tag{4}$$

where q denotes one dimensional Bloch parameter or the wave number, which is associated to the wavelength β as $\beta=2\pi/q$, l is characteristics unit cell the length and i is $\sqrt{-1}$. The expression

iql in equation (4) is represented as propagation constant μ. Similar relations are applied to shear forces and bending moments.

The constants A, B, C and D in equation (3) are determined by using the beam boundary conditions depicted in Figure 3(c), which are subsequently used to find out the expression of shear forces S and bending moments M on two sides of generic node j. The dynamic compliances[23,24] at $x = 0$ and $x = l$ for $\phi_0 = 0$ and $y_0 = 1$, are,

$$S_0' = \frac{\lambda^3 EI[\sin(\lambda l) + \sinh(\lambda l)]}{1 - \cos(\lambda l)\cosh(\lambda l)}$$

$$S_l' = \frac{\lambda^3 EI[\cosh(\lambda l)\ \sin(\lambda l) + \cos(\lambda l)\sinh(\lambda l)]}{1 - \cos(\lambda l)\cosh(\lambda l)}$$

$$M_0' = \frac{\lambda^2 EI[\cos(\lambda l) - \cosh(\lambda l)]}{1 - \cos(\lambda l)\cosh(\lambda l)} \tag{5}$$

$$M_l' = \frac{\lambda^2 EI[\sinh(\lambda l)\sin(\lambda l)]}{1 - \cos(\lambda l)\cosh(\lambda l)}$$

and the compliances for $\psi_0 = 1$ and $y_0 = 0$ are read as

$$S_0'' = \frac{-\lambda^2 EI[\cosh(\lambda l) - \cos(\lambda l)]}{1 - \cos(\lambda l)\cosh(\lambda l)}$$

$$S_l'' = \frac{-\lambda^2 EI[\sinh(\lambda l)\sin(\lambda l)]}{1 - \cos(\lambda l)\cosh(\lambda l)}$$

$$M_0'' = \frac{-\lambda EI[\sin(\lambda l) - \sinh(\lambda l)]}{1 - \cos(\lambda l)\cosh(\lambda l)} \tag{6}$$

$$M_l'' = \frac{-\lambda EI[\cosh(\lambda l)\ \sin(\lambda l) - \cos(\lambda l)\sinh(\lambda l)]}{1 - \cos(\lambda l)\cosh(\lambda l)}$$

Based on Figure 3(b), the expression of S and M at two sides of generic node j are determined as

$$S^- = -S_0' y_j e^{-iql} + S_l' y_j + S_0'' \phi_j^+ e^{-iql} + S_l'' \phi_j^-$$

$$S^+ = S_0' y_j e^{iql} - S_l' y_j + S_0'' \phi_j^- e^{iql} + S_l'' \phi_j^+$$

$$M^- = M_0' y_j e^{-iql} + M_l' y_j - M_0'' \phi_j^+ e^{-iql} + M_l'' \phi_j^- \tag{7}$$

$$M^+ = M_0' y_j e^{iql} + M_l' y_j + M_0'' \phi_j^- e^{iql} - M_l'' \phi_j^+$$

The kinematic compatibility condition at node j entails,

$$\phi_j^+ = \phi_j^- \tag{8}$$

and the equilibrium condition at node j (Figure 3(d)) yields the forces and bending moments equations as,

$$M^+ = M^-$$
$$S^+ = S^- + (K_R - M\omega^2)y_j \tag{9}$$

where, M and K_R respectively refers to the lumped mass and stiffness of the rack column.

equations (7)-(9) provides a system of the linear homogeneous equations in term of ϕ_j^-, ϕ_j^+ and y_j as,

$$\phi_j^- - \phi_j^+ = 0 \tag{10}$$

$$(M_0'' e^{iql} - M_l'')\phi_j^- + (M_0'' e^{-iql} - M_l'')\phi_j^+ + [2iM_0' \sin(ql)]y_j = 0 \tag{11}$$

$$(S_0'' e^{iql} - S_l'')\phi_j^- + (S_l'' - S_0'' e^{-iql})\phi_j^+ + [2S_0' \cos(ql) - 2S_l' - K_R + M\omega^2]y_j = 0 \tag{12}$$

Equations (10)-(12) can be expressed as,

$$Du = 0 \tag{13}$$

where, $u = (\phi_j^-,\ \phi_j^+, y_j)^T$ and

$$D = \begin{bmatrix} 1 & -1 & 0 \\ M_0'' e^{iql} - M_l'' & M_0'' e^{-iql} - M_l'' & 2iM_0' \sin(ql) \\ S_0'' e^{iql} - S_l'' & S_l'' - S_0'' e^{-iql} & 2S_0' \cos(ql) - 2S_l' - K_R + M\omega^2 \end{bmatrix}$$

For u to have a non-trivial solution, the determinant of D should be zero,

$$\begin{vmatrix} 1 & -1 & 0 \\ M_0'' e^{iql} - M_l'' & M_0'' e^{-iql} - M_l'' & 2iM_0' \sin(ql) \\ S_0'' e^{iql} - S_l'' & S_l'' - S_0'' e^{-iql} & 2S_0' \cos(ql) - 2S_l' - K_R + M\omega^2 \end{vmatrix} = 0 \tag{14}$$

A further solution of equation (14) yields the dispersion relation for the infinite periodic piping system as,

$$[4M_0' S_0'' \sin^2(ql)] + [2S_0' \cos(ql) - 2S_l' - K_R + M\omega^2][2M_0'' \cos(ql) - 2M_l''] = 0 \tag{15}$$

By inserting compliance coefficients relations in equation (15), the dispersion relation in term of frequency ω (i.e., part of λ) and the propagation constant μ is obtained as,

$$
\begin{aligned}
&[\{\cosh(\lambda l)-\cos(\lambda l)\}]^2-\{\sinh^2(\lambda l)-\sin^2(\lambda l)\}]\cosh^2\mu\\
&+\Bigg[\{\sinh(\lambda l)-\sin(\lambda l)\}\{\cosh(\lambda l)\ \sin(\lambda l)+\cos(\lambda l)\sinh(\lambda l)\}\\
&-\{\cosh(\lambda l)\ \sin(\lambda l)-\cos(\lambda l)\sinh(\lambda l)\}\{\sin(\lambda l)+\sinh(\lambda l)\}\\
&+\frac{\{\sinh(\lambda l)-\sin(\lambda l)\}\{1-\cos(\lambda l)\cosh(\lambda l)\}\{K-M\omega^2\}}{2EI\lambda^3}\Bigg]\cosh\mu\\
&+\Bigg[\{\sin^2(\lambda l)\cosh^2(\lambda l)-\cos^2(\lambda l)\sinh^2(\lambda l)\}-\{\cosh(\lambda l)-\cos(\lambda l)\}^2\\
&+\frac{\{\cosh(\lambda l)\ \sin(\lambda l)-\cos(\lambda l)\sinh(\lambda l)\}\{1-\cos(\lambda l)\cosh(\lambda l)\}\{K-M\omega^2\}}{2EI\lambda^3}\Bigg]=0
\end{aligned}
\tag{16}
$$

The solution of equation (16) yields two distinct pairs of μ: $\pm\mu_1$ and $\pm\mu_2$ for each frequency ω. Two signs of each pair of μ represent the same characteristic waves travelling in opposite direction. Based on the characteristics of μ, waves are defined in three ways. For purely real μ, the amplitude of wave decayed in the adjacent unit cells, such a wave is described as an evanescent wave. Conversely, if μ is purely imaginary, a wave travels freely in the structure without attenuation. For a complex μ, some waves get attenuated and remaining pass freely through the structure, thus resulting in both stop and pass bands in a band structure.

FE modelling of finite periodic piping system

To validate the analytical dispersion relations, the finite element (FE) models of pipe *P* with different type of support conditions are developed using an Euler-Bernoulli beam (BEAM4) available in ANSYS APDL 19.0. The linear spring and lumped mass are modelled using COMBIN14 and MASS21 elements, respectively. To study the transmission behaviour of waves in *P*, a unit amplitude rotation in the form $\phi_{i/p}e^{\mathrm{i}2\pi ft}$ ($f=\omega/2\pi$) is imposed on the leftmost end of the pipe and the output response $\phi_{o/p}(f)$ is computed at the rightmost end. In pipe *P*, the vibration transmission behaviour in decibel form is expressed by FRF (dB), and is defined as,

$$FRF = 20\ log_{10}\left|\frac{\phi_{o/p}(f)}{\phi_{i/p}(f)}\right| \tag{17}$$

A finite structure can approximate the realistic scenario of an infinite structure, such that band gaps in both can occur within the same frequency regime if sufficiently large number of unit cells are considered. The attenuation behaviour of waves in band gaps highly depends upon the number of unit cells available in the structure. Since, the modelling of an infinite periodic structure is not straightforward, therefore, 40 unit cells are used.

Results and discussion

In this section, wave propagation in an infinite and finite periodic piping system is carried out and discussed. Firstly, wave propagation behaviour in Model #A, Model #B and Model #C without resonator is investigated analytically and numerically. Further, propagation of wave in all the three

models when coupled with a 2DoF resonator is computed numerically. The influence of resonator properties on band gaps is studied at last.

Dispersion characteristics of an infinite periodic piping system

To study the flexural waves propagation behaviour in P, a simplified model illustrated in Figure 2(a) is considered. In this regard, a pipe-rack structure made by the concrete of a class C50/40 as shown in Figure 1, is used. The distance between two columns along the length of the pipe is 6 m. There are two storeys in each frame. The height of lower and upper storey from the ground is 5.3 m and 7.3 m, respectively. The cross-sectional area of each column is 600 mm^2.The rack contains forty frames whose first ten frames are depicted in Figure 1. A FE model of rack and it's an equivalent model with lumped mass M and linear spring K_R corresponding to Figure 2(a) are developed in such a way that they carry same dynamic characteristics for the first lateral mode. The first mode entails at a frequency of 4.42 Hz, based on that the values of K_R and M is computed to be 18 $E6$ N/m and 23 $E3$ kg, respectively.
In the calculation, the following geometric and material properties of P are used:
Outer radius $R_0 = 203.20\,mm$, thickness $t = 7.92\,mm$, length $l = 6\,m$, density $\rho = 7800\,kg/m^3$ and Young's modulus $E = 200\,GPa$.

Based on equation (16), the variation of imaginary and real parts of μ with frequency f is calculated and are represented in Figures 4(a) and 4(b), respectively. The frequency ranges of three band gaps are $[0 - 4.42]\,Hz$, $[5.45 - 31.25]\,Hz$ and $[71.25 - 123.25]\,Hz$, respectively, and are highlighted by shaded areas. The FRF (from equation (20)) shown in Figure 4(c) represents the FE model results. The Re(μ) and FRF report the attenuation characteristics of the wave and are indicating good agreement with each other, while Im(μ) represents the propagation characteristics of waves. The first order band gap is due to the local resonance of rack, while remaining two are by spatial periodicity. Thus, two types of band gaps appear in the dispersion curves.

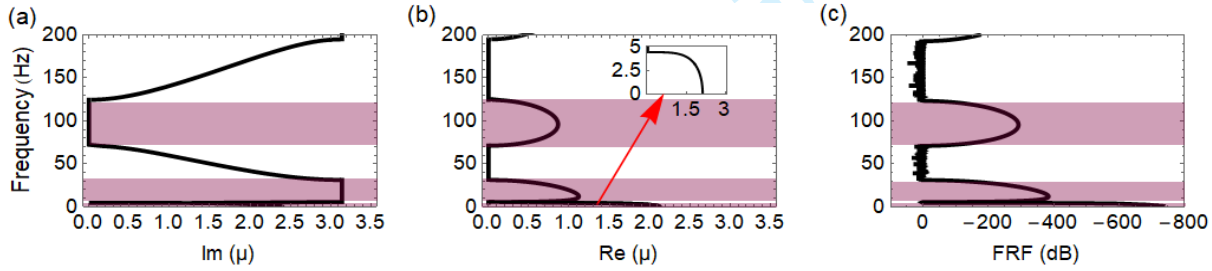

Figure 4. Dispersion curves and vibration transmission behaviour of Model #A: (a) Imaginary part of (μ); (b) Real part of (μ); and (c) FRF (dB).

Substitution of $M = 0$ and $K_R \to \infty$ in equation (16) approaches to an extreme case of P with simple supports (i.e., Model #B), and the resulting expression becomes,

$$\cosh(\mu) = \frac{\cosh(\delta l)\ \sin(\delta l) - \cos(\delta l)\sinh(\delta l)}{\sin(\delta l) - \sinh(\delta l)} \qquad (18)$$

The above expression can also be found in the literature[3].

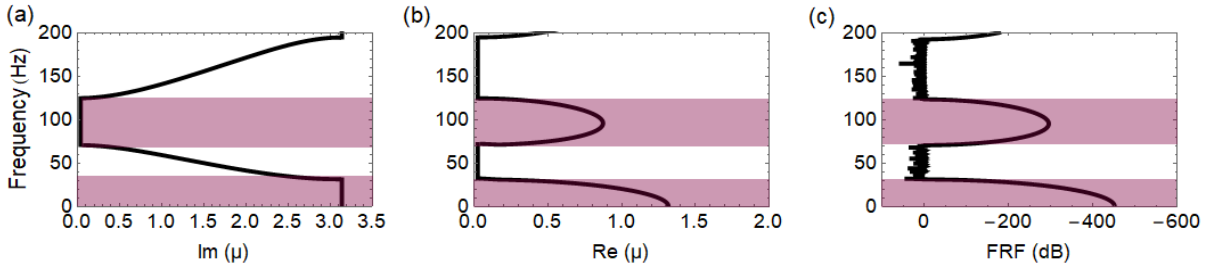

Figure 5. Dispersion curves and vibration transmission behaviour of Model #B: (a) Imaginary part of (μ); (b) Real part of (μ); and (c) FRF (dB).

The imaginary and real part of μ calculated based on equation (18) are respectively shown in Figures 5(a) and 5(b), while Figure 5(c) reports to FRF of P. The same frequency range is considered here as of Model #A, two band gaps are obtained with the frequency range of $[0 - 31.25]\ Hz$ and $[71.25 - 123.25]\ Hz$ which are shown by shaded areas in Figure 5. However, the remaining frequencies belong to the pass bands. Both analytical and numerical results show good accordance with each other. In this case, only Bragg band gaps are obtained.

When $K_R \to 0$, the dispersion relation derived in equation (16) entails a particular case of homogeneous P without support (i.e., Model #C), and the dispersion relation changes to,

$$\cosh^2\mu - [\cos(\delta l) + \cosh(\delta l)]\cos\mu + \cos(\delta l)\cosh(\delta l) = 0 \qquad (19)$$

Equation (19) can also be found in[25], and is used to calculate the dispersion curves for Model #C, which are depicted in Figures 6(a) and 6(b), respectively, and are verified with FRF given in Figure 6(c). It is observed that no band gap is obtained for this case, and thus the waves of all frequencies can freely travel in P.

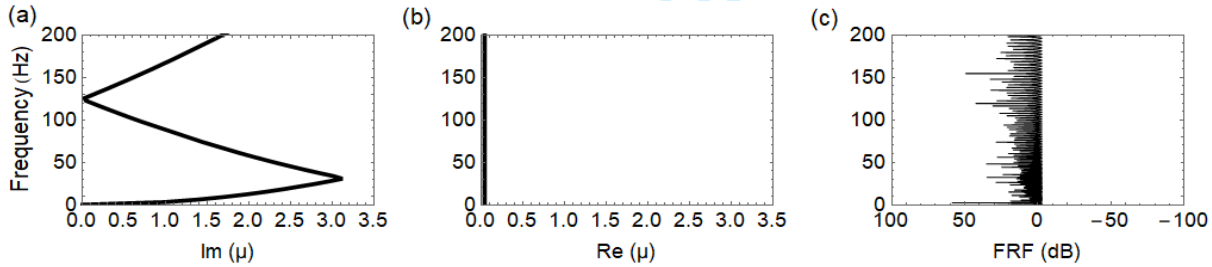

Figure 6. Dispersion curves and vibration transmission behaviour of Model #C: (a) Imaginary part of (μ); (b) Real part of (μ); and (c) FRF (dB).

Vibration transmission in P attached with 2DoF resonator

The flexural vibration characteristics in P without a resonator have been investigated in the previous section for the three models. It is apparent from the results of Model #A, the first pass band is extremely narrow, but the other two are wide pass bands. In case of Model #B, both pass bands are large, while Model #C shows only pass band. Hence, waves within these pass bands can travel freely through the pipe without any attenuation, thus, it is essential to control these pass bands to protect the piping system from higher frequency vibrations. As, in case of Model #A and

Model #B, it is not possible to control two pass bands with a SDoF resonator, therefore, a 2DoF resonator is used. Further, same resonator is utilized with Model #C.

The flexural wave propagation study of P with a 2DoF resonator is carried out and the corresponding model is depicted in Figure 2(b). The resonator comprises of the two masses: m_1 and m_2, two springs with stiffnesses: k_1 and k_2 and two viscous dampers with damping coefficients c_1 and c_2. The properties of the 2DoF resonator are adopted such that the second and third pass band of Model #A and the first and second pass band of Model #B can be controlled. If the mass of each unit span of P is M_P, and η is a mass ratio, then the parameters of a resonator are considered as,

$m_1 = m_2 = \eta M_P, \eta = 0.16, M_P = \rho A l,\ k_2/k_1 = 0.1\ , k_1 = 5.2E7\ N/m\ ,\ c_2/c_1 = 0.67, c_1 = 1.5E4.$

When $c_1 = c_2 = 0$, and the pipe is considered to be undamped, then two additional band gaps are emerged in the FRF. These two new band gaps are due to the local resonances of resonator and open around its natural frequencies. For Model #A, the frequency range of five band gaps are obtained as $[0 - 4.4]\ Hz$, $[5.5 - 22.75]\ Hz$, $[36.25 - 47.75]\ Hz$, $[66.25 - 123.25]\ Hz$ and $[150.75 - 162.5]\ Hz$, respectively. In FRF, Ist, IIIrd and Vth band gaps are due to local resonances, Ist because of the rack while IIIrd and Vth are due to the 2DoF resonator. However, IInd and IVth are Bragg band gaps. For Model #B, the four respective band gap frequency ranges are $[0 - 22.75]\ Hz$, $[36 - 48]\ Hz$, $[66.50 - 123.50]\ Hz$ and $[151 - 162.75]\ Hz$, respectively. Similarly for Model #C, four band gaps are $[23 - 31]\ Hz$, $[42.5 - 49]\ Hz$, $[104.25 - 124]\ Hz$ and $[149 - 177.25]\ Hz$, respectively. In FRF of Model #B and Model #C, the Ist and IIIrd band gaps are the Bragg band gaps while remaining two (i.e., IInd and IVth) are LR band gaps. The obtained band gaps for the three models are represented by shaded areas in Figures 7(a), 7(b) and 7(c), respectively.

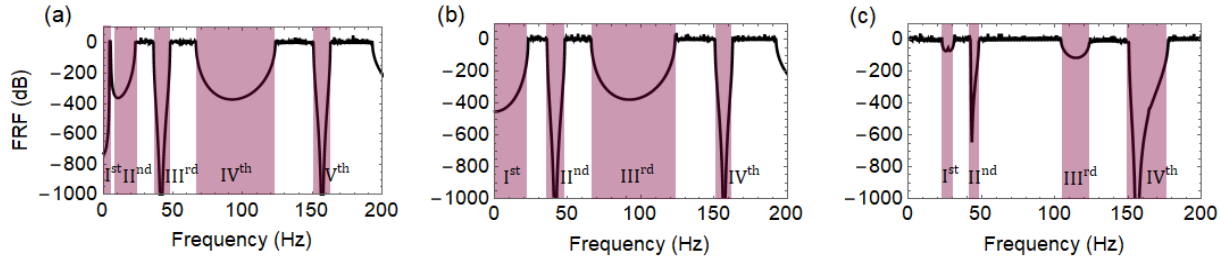

Figure 7. FRF (dB) of different models: (a) Model #A ; (b) Model #B; and (c) Model #C.

Parametric study of resonator properties on band gaps

The influence of various parameters of a 2DoF resonator on band gaps is investigated in depth, including mass ratio η, spring stiffnesses k_1, k_2 and the damping coefficients c_1, c_2. The analysis for various resonator parameters is compared against the results presented in Figure 7 for the original values given in the previous section. In this regard, only a particular parameter is changed while others remain constant. For a comparative study, two values are assumed, one lower and the other higher than the original value of the resonator.

Firstly, the effect of η on band gaps is presented in Figure (8) for the two selected values of 12% and 20%. It is observed that the starting and terminal frequencies of LR band gaps are affected

with the increase of η, and shift to the low-frequency regime. Consequently, the position of both LR band gaps moves to the low-frequency range, and their widths also increases with η. The Vth band gap of Model #A and IVth (refer Figure 7 for the order of band gaps) band gap of Model #B and Model #C realize significant influence of η as compared to the other LR band gap of the resonator. However, the starting frequency of the Bragg band gap, which falls between two LR band gaps of the resonator, slightly shifts to the left while the terminal frequency remains same. Consequently, the Bragg band gap gets wider. Although, the other Bragg band gap remains same in all the three models, which can be observed in the FRF as shown in Figure 8.

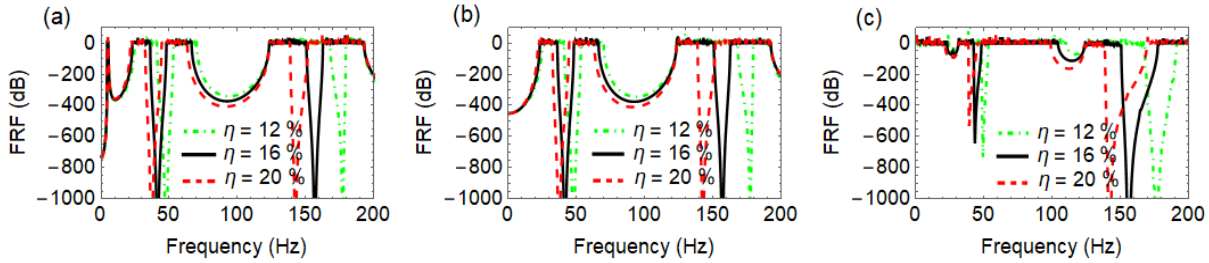

Figure 8. Influence of mass ratio (η) on band gaps: (a) FRF of Model #A ; (b) FRF of Model #B; and (c) FRF of Model #C.

Figure 9 shows the effect of k_1 and k_2 on band gaps for Model #A, while Figure 10 and 11 correspond to the results for Model #B and Model #C, respectively. Two values of k_1 are selected as, $3.7E7\ N/m$ and $6.7E7\ N/m$, and values of k_2 are assumed to be $2.2E6\ N/m$ and $8.2E6\ N/m$, respectively. It can be noticed in Figure 9(a) that an increase in k_1 leads to a higher starting and terminal frequencies of the Vth band gap and an increase in its width. However, all other band gaps do not change.

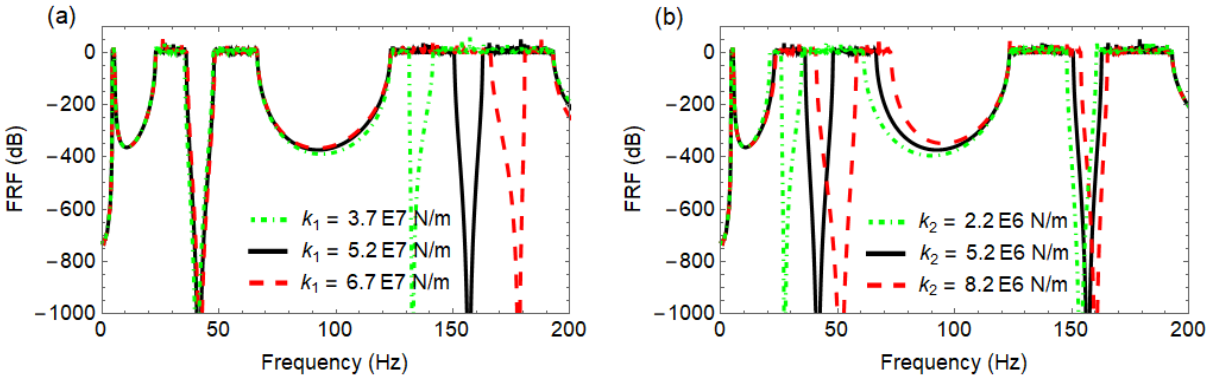

Figure 9. Influence of resonator stiffness on band gaps for Model #A: (a) effect of k_1; and (b) effect of k_2.

However, with the increase of k_2, both LR band gaps get influenced: their positions shift to a higher frequency range and bandwidth increases. The IInd band gap (Bragg type) has a negligible effect on the band edge frequencies but starting frequency of the IVth band gap (Bragg type) shifts much to a higher frequency while terminal frequency does not change. Consequently, the width of IVth band gap decreases significantly. Similar effects of k_1 and k_2 are observed on both types of band gaps for Model #B and can be seen in Figure 10.

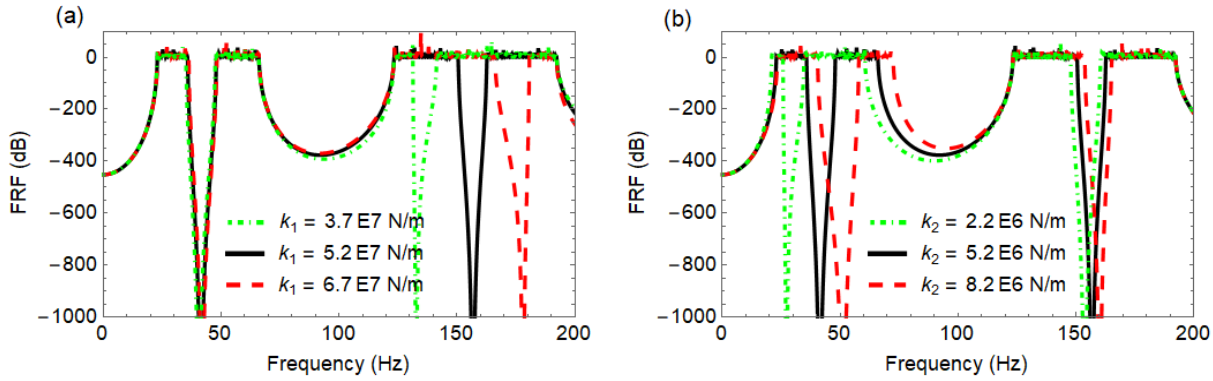

Figure 10. Influence of resonator stiffness on band gaps for Model #B: (a) effect of k_1; and (b) effect of k_2.

Figure 11 reveals the influence of the variation of k_1 and k_2 on band gaps for Model #C. It demonstrates that the increase in k_1 highly influences both starting and terminal frequencies of IVth band gap and shifts the position towards right and also increases the bandwidth. However, starting frequency of the IIIrd band gap moves to right and the terminal frequency remains same. As a result, the width of this band gap decreases. The frequency range of Ist and IInd band gaps does not change with k_1. When k_2 is increased, the location of Ist and IInd band gaps is highly influenced , while effect on IIIrd and IVth band gaps is insignificant, which can be observed in Figure 11(b). For $k_2 = 2.2E6\,N/m$, the LR band gap emerges before the Bragg band gap, while for $k_2 = 5.2E6\,N/m$ and $8.2E6\,N/m$, the LR and Bragg band gap interchange their positions, and can be easily noticed in Figure 11(c).

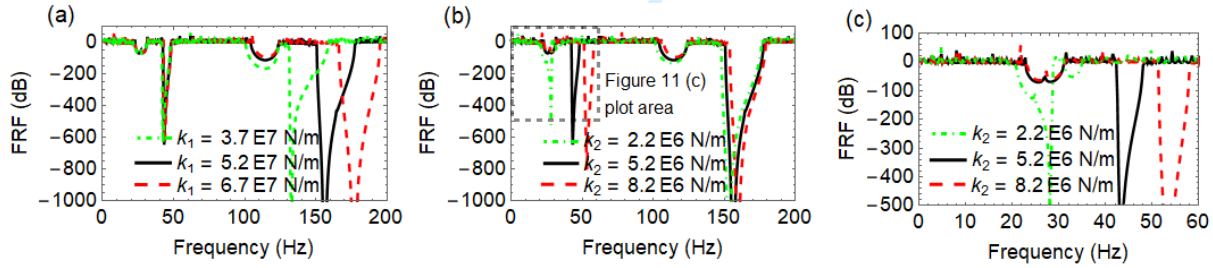

Figure 11. Influence of resonator stiffness on band gaps for Model #C: (a) effect of k_1; and (b) effect of k_2.

Figure 12 shows the influence of various damping values on band gaps when a 2DoF resonator is coupled with P, three scenarios with different damping values are investigated in all the three models; (i) P and resonator both are undamped, (ii) P is damped ($\xi = 0.02$) and the resonator is undamped ($k_1 = 5.20E7$, $c_1 = 0$ and $k_2 = 5.2E6$, $c_2 = 0$); and (iii) P ($\xi = 0.02$) and resonator both are damped ($k_1 = 5.2E7$, $c_1 = 1.5E4$ and $k_2 = 5.2E6$, $c_2 = 1.0E4$). The FRF of different models corresponding to the above three cases are reported in Figure 12.

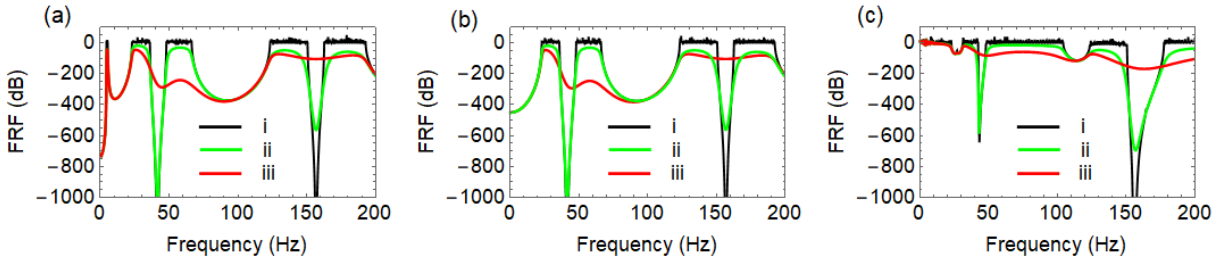

Figure 12. FRF of P attached with 2DoF LLR for different damping values: (a) Model #A ; (b) Model #B; and (c) Model #C.

In case (i), the band gaps and transmission peaks are apparent, while in case (ii), the edges of band gaps slightly deform and the transmission peaks lower in the respective pass bands. However, case (iii) shows that high damping vanishes the band gaps and leads to a significant reduction in the response which can be observed in Figure 12.

Conclusions

The propagation characteristics of lateral flexural waves in a periodic piping system without and with resonators was investigated analytically and numerically. Periodic structure theory was employed to obtain the analytical dispersion relation of periodic piping system which was subsequently verified by the FE model. Additionally, the dispersion relations for two different cases were also evaluated.

The results of Model #A revealed that the flexibility of rack introduces a narrow LR band gap starting from 0 Hz, and thus both types of band gaps coexist in the dispersion curves. Conversely, in case of Model #B, only Bragg band gaps are emerged. Although, no band gap is found in case of Model #C.

Further, wave propagation in P with 2DoF resonators was investigated. FRF of P with 2DoF resonator displays two new LR band gaps which open around its natural frequencies. Thus, waves in two targeted pass bands of Model #A and Model #B can be controlled effectively. However, the wave filtering capability of Model #C is highly increased, as without resonators no band gap is obtained in this case.

Moreover, the influence of resonator parameters, the mass ratio η, resonator stiffnesses k_1, k_2 and the damping coefficients c_1, c_2 on band gap characteristics was investigated for the three models. The FRF of different models convey the information about change in the starting and terminal frequencies and also the position, width and disappearance of both types of band gaps when any particular parameter is changed.

The study carried out in this paper is promising in flexural vibration control of the periodic piping system with different boundary conditions and may be helpful in the design of resonator. Introduction of a nonlinear mechanism in the modelling of support and resonator can be the area of further research.

Declaration of conflicting interests

The author(s) declared no potential conflicts of interest with respect to the research, authorship, and/or publication of this article.

Funding
This work was supported from Science and Engineering Research Board, Govt. of India, core research grant CRG/2018/002539 (SER-1332-MID) for the first and second author. This work received support from the Italian Ministry of Education, University and Research (MIUR) in the frame of the 'Departments of Excellence' (grant L 232/2016) for the last author.

References

1. Singh K and Mallik AK. Wave propagation and vibration response of a periodically supported pipe conveying fluid. *J Sound Vib* 1977; 54: 55–66.
2. Koo GH and Park YS. Vibration reduction by using periodic supports in a piping system. *J Sound Vib* 1998; 210: 53–68.
3. Gupta GS. Natural flexural waves and the normal modes of periodically supported beams and plates. *J Sound Vib* 1970; 13: 89–101.
4. Mead DJ. Free wave propagation in periodically supported, infinite beams. *J. Sound Vib* 1970; 11: 181–197.
5. Liu L and Hussein MI. Wave motion in periodic flexural beams and characterization of the transition between bragg scattering and local resonance. *J Appl Mech Trans ASME* 2012; 79: 1–17.
6. Liu ZY, Zhang XX, Mao YW, et al. Locally resonant sonic materials. *Science* 2000; 289: 1734–1736.
7. Sonti VR and Narayana TSS. Propagation constants from the response of a finite periodic beam. *Noise Control Eng J* 2006; 54: 194–200.
8. Gupta GS. Natural frequencies of periodic skin-stringer structures using a wave approach. *J Sound Vib* 1971; 16: 567–580.
9. Huang GL and Sun CT. Band Gaps in a multiresonator acoustic metamaterial. *J Vib Acoust* 2010; 132: 1–6.
10. Yu D, Wen J, Zhao H, et al. Vibration reduction by using the idea of phononic crystals in a pipe-conveying fluid. *J Sound Vib* 2008; 318: 193–205.
11. Yu D, Wen J, Shen H, et al. Propagation of steady-state vibration in periodic pipes conveying fluid on elastic foundations with external moving loads. *Phys Lett Sec A Gen At Solid State Phys* 2012; 376: 3417–3422 .
12. Hu B, Zhu F, Yu D, et al. Impact vibration properties of locally resonant fluid-conveying pipes. *Chinese Phys B* 2020; 29: 0–9.
13. Liu Y, Yu D, Zhao H, et al. Design guidelines for flexural wave attenuation of slender beams with local resonators. *Phys Lett Sect A Gen At Solid State Phys* 2007; 362: 344–347.
14. Xiao Y, Wen J, Yu D. et al. Flexural wave propagation in beams with periodically attached vibration absorbers: Band-gap behavior and band formation mechanisms. *J Sound Vib* 2013; 332: 867–893.
15. Zhou X, Wang J, Wang, R. et al. Band gaps in grid structure with periodic local resonator subsystems. *Mod Phys Lett B* 2017; 31: 1–10.
16. Yu D, Liu Y, Wang G, et al. Low frequency torsional vibration gaps in the shaft with locally resonant structures. *Phys Lett Sect A Gen At Solid State Phys* 2006; 348: 410–415.
17. Song Y, Wen J, Yu D, et al Analysis and enhancement of torsional vibration stopbands in a periodic shaft system. *J Phys D. Appl Phys* 2013; 46: 145306.
18. Nobrega ED, Gautier F, Pelat A, et al. Vibration band gaps for elastic metamaterial rods

using wave finite element method. *Mech Syst Signal Process* 2016; 79: 192–202.
19. Wang Z, Zhang P and Zhang Y. Locally resonant band gaps in flexural vibrations of a Timoshenko beam with periodically attached multioscillators. *Math Probl Eng* 2013; 2013:146975.
20. Xiao Y, Wen J and Wen X. Longitudinal wave band gaps in metamaterial-based elastic rods containing multi-degree-of-freedom resonators. *New J Phys* 2012; 14:033042.
21. Floquet G. On the Linear Differential Equations With Periodic Coefficients. *Ann Sci l'École Norm Supérieure* 1883; 12: 47–88.
22. Bloch F. Über die Quantenmechanik der Elektronen in Kristallgittern. *Zeitschrift für Phys* 1928; 52: 555–600.
23. Clough RW and Penzien J. *Dynamics of Structure*. McGraw-Hill, 1975.
24. Brun M, Movchan AB and Slepyan LI. Transition wave in a supported heavy beam. *J Mech Phy. Solids* 2013; 61, 2067–2085.
25. Cremer L. and Heckl M. *Structure-Borne Sound*. Springer-Verlag Berlin Heidelberg GmbH, 1988.